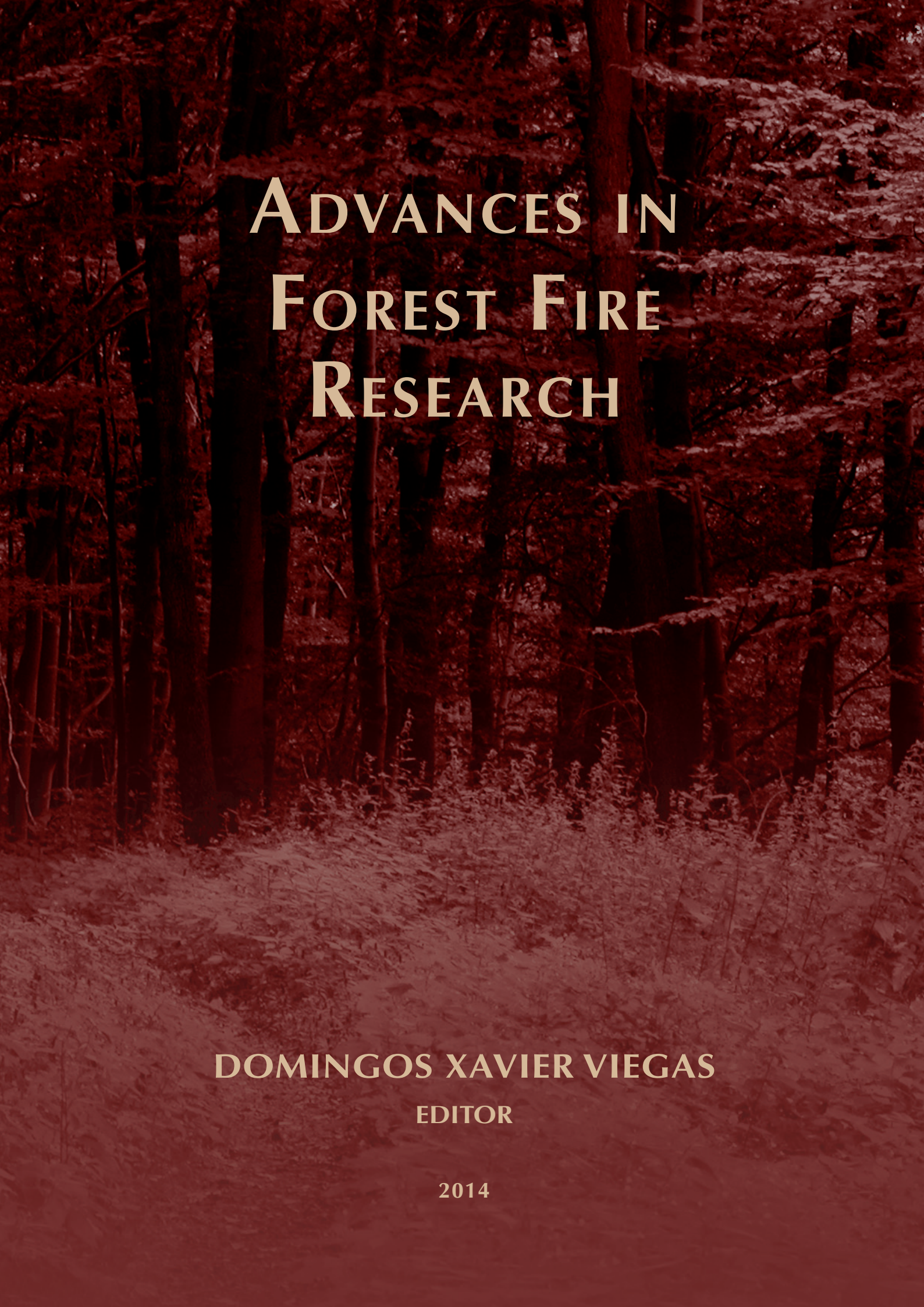

Advances in Forest Fire Research

DOMINGOS XAVIER VIEGAS

EDITOR

2014

Studying wildland fire spread using stationary fires

D.J. Gorham[a], R. Hakes[a], A.V. Singh[a], J. Forthofer[b], J. Cohen[b], S. McAllister[b], M.A. Finney[b] and M.J. Gollner[a]

[a] *Department of Fire Protection Engineering, University of Maryland, College Park, MD 20742, USA. dgorham1@umd.edu, mgollner@umd.edu*
[b] *US Forest Service, Missoula Fire Sciences Lab, Missoula, MT 59808, USA. jaforthofer@fs.fed.us, mfinney@fs.fed.us*

Abstract
Experiments were performed using stationary gas burners and liquid fuel-soaked wicks to study fundamental wildland fire behaviour, including unsteady flame heating. These experiments were motivated by observations of instabilities in spreading fire experiments that suggest they play a critical role in fire spread. Stationary fire experiments in forced flow and on inclined surfaces exhibited instabilities similar to those observed in spreading fires but allowed for more detailed analysis of the mechanisms responsible. Large scale inclined experiments were performed using an ethylene gas-fed burner at angles from 10 to 60 degrees. Forced flow experiments were performed on liquid-soaked wicks and small scale gas burners at wind speeds from 0.2 to 3 $\mathbf{ms^{-1}}$. Results presented include observations of the general flame structure, including streamwise streak spacing and flame fluctuation frequencies which relate to instabilities observed in large spreading experiments. A description and correlations of flame geometry, useful for predictions of wildland fire spread are also presented.

Keywords*: wildland fire, inclined flame spread, diffusion flame, flame pulsation*

1. Introduction

Predicting the rate of spread (ROS) of large wildland fires is of critical importance for operational firefighting, prescribed burning, and calculating future wildfire potential. Currently, most of these models are based upon correlations derived from experiments performed in the 1970's by Rothermel, Anderson and others (Finney *et al*. 2013a). While these correlations provided a "leap forward" in the prediction of a steady ROS, they failed to capture essential physics and therefore break down under extreme wind, topographic, and other conditions (Finney *et al*. 2013b). A considerable amount of effort is therefore being invested towards better understanding this fire behaviour, especially the mechanisms of heating to fuel particles. While it has proven difficult to study these phenomena in some large-scale spreading fires, a series of stationary, scaled experiments have been designed to determine the underlying physics that occur during fire spread.

Recent experiments of flame spread in discrete fuel beds have revealed the presence of buoyant instabilities which may lead to increased convective heating of fuel particles (Finney *et al*. 2013a). Unfortunately, detailed fluid dynamics and convective heating measurements in spreading fires remain difficult to capture because of the moving burning region of the fire. This is compounded by changes in the flame front and fuel burnout with time, causing non-steady burning rates and dynamic fire behaviour that require dozens of expensive, large scale fire experiments to investigate. Stationary burners have long been used to study fires in the built environment (de Ris and Orloff 1975), therefore they offer an ideal configuration to study non-steady fire effects in a thorough, statistical manner, in essence capturing a snapshot of a moving fire front. Experiments here show these stationary burning regions contain two buoyant instabilities which are similar to spreading fires, appropriately scaling with macro-features of large spreading fires, however they provide enhanced measurement capabilities (Finney *et al*. 2013a).

2. Motivation

Recent studies of spreading fires in the 3×3 m wind tunnel at the Missoula Fire Science Laboratory have shown coherent structures that form in the streamwise direction of the flow as well as spanwise fluctuations that propagate to the downstream edge of the flame zone contributing to fuel heating. The highly spatially-uniform fuel beds used in these experiments allowed for the observation of these structures with more repeatable results than previous efforts (Finney *et al*. 2013a). The results suggest that flame spread in fine fuel beds is driven by non-steady convective heating and intermittent flame contact on fuel particles. These heating characteristics were measured using micro thermocouple arrays and high speed video. The travelling flaming region, however, made it difficult to carefully study these properties, such as a statistical analysis of these features which appear stochastically in the flow. A technique was therefore needed that could study these new instabilities and other general structures of propagating wildfires in a small-scale configuration that can be utilized over long times.

Figure 1. Photos demonstrating the scales over which coherent streaks and flame towers have been observed. (a) Inclined gas burner, $L_f \approx 0.2$ m, (b) Comb burn experiments in 3×3 m wind tunnel, $L_f \approx 2$ m, and (c) Canadian Crown fire experiments, $L_f \approx 30$ m (Clark et al. 1999).

A stationary, non-spreading fire was chosen as it allows for a thorough statistical analysis of the flame structure. Long-duration experiments allow for a large sample size and more control over variations in experimental parameters, such as decoupling the heat-release rate of the fire from flow conditions, unachievable in spreading fires. The flame zone depth in the direction of fire spread can also be carefully adjusted via the size of the burner. High speed video and micro thermocouples are useful on these fires to reveal and track buoyant instabilities in the fire flow which resemble those appearing in spatially-uniform fuel beds. The same intermittent heating observed in the fuel bed experiments were observed in the stationary burner, but with the ability to collect a larger data set. Other modifications to the flow field, such as the incoming boundary layer thickness is also adaptable in these small scale experiments.

3. Methods

3.1. Experimental Setup

Forced-flow experiments were performed at both the USDA Forest Service's Missoula Fire Science Laboratory and a specially-designed 30 centimeter cross section wind tunnel at the University of Maryland's Fire Phenomenon Laboratory (UMD). In Missoula, a propane burner was constructed in the laboratory, using sintered metal as the porous burner surface which measured approximately 30 by 25 cm. A volumetric flow meter was used to measure the flow rate of propane gas into the burner, and experiments were conducted at fire sizes of 7.5, 10.9, and 15.1 kW. Ceramic insulation board was placed around the burner so as to make a continuous flat, inert surface to limit side-air entrainment. The apparatus was tested in a low-speed tunnel, 3×3 m cross section, at free-stream velocities of 0.22, 0.44, 0.67, 0.89, 1.11, and 1.34 ms^{-1}. Side view video was captured with a Phantom brand high-speed camera at 120 frames per second.

At UMD, a laminar wind blower was designed and built for uniform forced flow combustion experiments. The wind blower was designed to pressurize a 0.75 cubic-meter plenum box with a centrifugal fan. The flow then travels through a converging section into a 30×30 cm rectangular duct into a mesh screen and honeycomb flow straightener. The flow travels another 1.35 m in the duct resulting in a fully-developed laminar boundary layer before it is exhausted at the outlet. The velocity profile of the boundary layer was measured along the centerline of the blower above the burner surface using a hot-wire anemometer. Measurements confirmed the blower is capable of repeatedly producing precise forced flow velocities between 0.6 and 4.8 ms^{-1} with turbulence intensities less than 3% at maximum velocities.

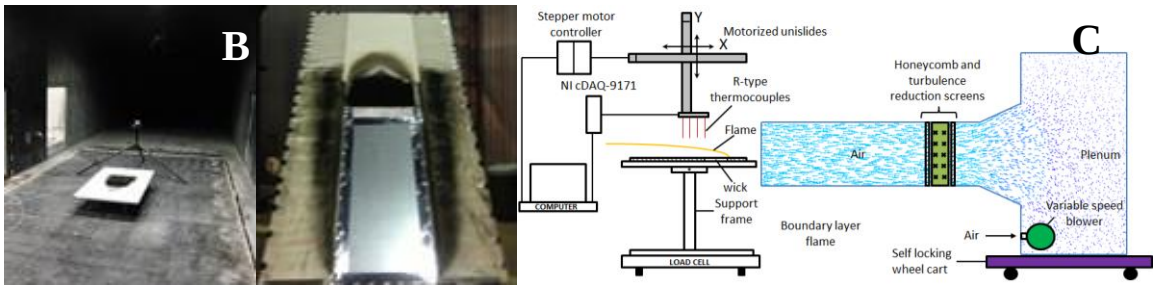

Figure 2: (A) Forced-flow gas burner in the Missoula 3×3 m wind tunnel, (B) Inclined gas burner at Missoula and (C) Forced flow configuration at UMD.

Large-scale inclined experiments were performed in Missoula on a gas burner flame wall repurposed from a vertical configuration (Jimenez *et al*. 2010). The retrofitted burner is rotatable so that experiments could be performed at inclination angles between 0 and 90 degrees relative to the ground. The width of the burner was 0.595 meters and the total burner surface height was 1.83 meters. To produce a line fire, sections of the burner were sealed so that gas flowed out of a ceramic plenum only above the exposed burner surface. The width of the line fire was fixed, based on the flame wall, but the depth of the burning region was changed between experiments by extending the amount of burner surface covered. Non-combustible surfaces were also attached to the top and sides of the flame wall in order to extend its length and width, minimizing side-air entrainment. Sidewalls were also considered for use, however it was found that at this scale such walls would induce the trench effect, drastically increasing flame lengths and flame attachment somewhat different than the open-fire behaviour trying to be studied here (Atkinson *et al*. 1995). A flush transition from the burner to the attachment section was ensured. Similar to vertical flame wall experiments (Finney *et al*. 2010), the burner was first purged with nitrogen and ethylene fuel was then introduced at a rate specified by the mass flow controller. Once the flame was fully developed across the exposed burner area, the flow of nitrogen was cut off.

3.2. Instrumentation

High-speed videography was used to capture digital images of the flame in all configurations from both the side and top view (Figure 1and 2). The side view camera was a Phantom, recording at 120 frames per second and a 1920×1080 pixel resolution, mounted on a tripod and tilted to give a parallel view of the flame relative to the attachment surface. The top-view camera was a high-speed Casio EFX-1, recording at 120 frames per second at a 640×480 pixel resolution, mounted on a tripod mounted to the bottom of the flame wall. This allowed for observation of the flame from the upstream edge at approximately a 45 degree angle. Micro-thermocouple arrays, similar to those used in spreading fire experiments (Finney *et al*. 2013a), were also placed downstream along the centerline of

the burner, raised 1 centimetre above the inert "unburnt fuel" surface with a spacing of 2 cm between thermocouples. Temperature measurements were sampled at a frequency of 120 Hertz.

4. Results

4.1. Mechanisms of Instability

In both spreading, forced flow (wind-driven) fires and stationary forced flow and inclined (sloped) experiments two dominant instabilities were observed. The first consisted of streamwise streaks, appearing as flame peaks and troughs when observed parallel to the direction of external flow (Figure 3). These structures resemble counter-rotating vortex pairs (Taylor-Görtler vortices) which form over concave surfaces (Saric 1994). The significance of these structures is that they splay flames downward into the fuel-bed, adding heating to the fuel surface that increases rates of flame spread. Similar structures have been observed in experiments on inclined heated surfaces with correspondingly increased rates of heat transfer noted (Jeschke and Beer 2001)**.** In stationary burner experiments, flame attachment was seen to occur downstream of the burner in both forced flow and inclined experiments, facilitating heating of "unburnt" fuel and thus simulating flame spread. Within this attachment region the flame front was also observed to pulse or burst further downstream, extending the direct flame contact zone with the unburnt fuel surface far beyond the mean flame front. The frequency of these observed pulsations were then extracted from oscillations of the flame location within this attachment region. This behavior is important as it could be similar to heating of fuel particles by direct flame contact which may be responsible for flame spread, as observed in larger scale experiments (Finney *et al*. 2013a).

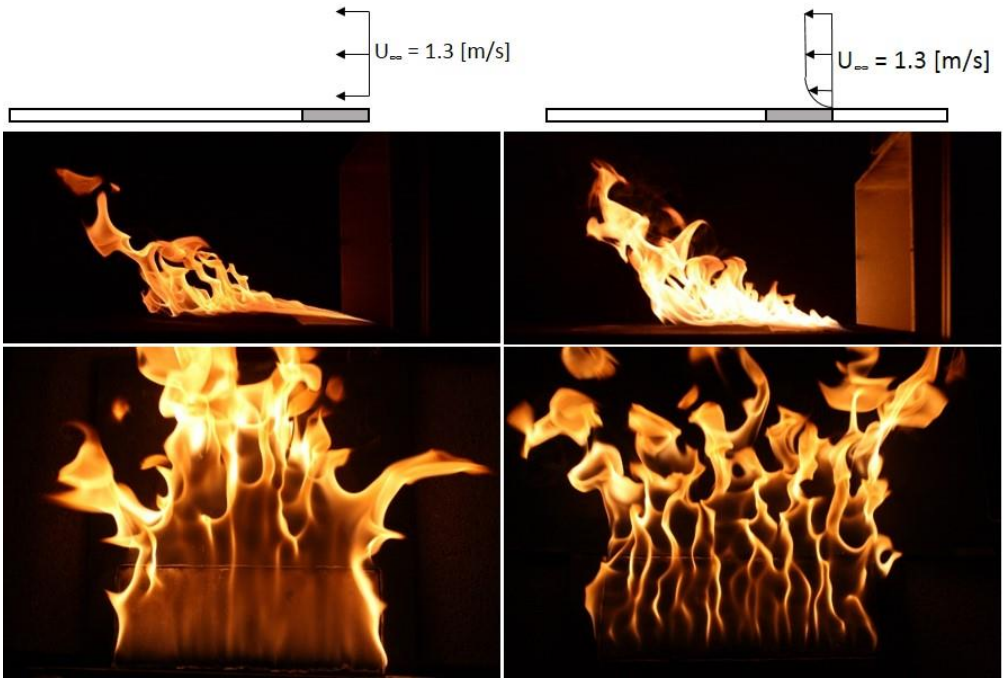

Figure 3. Boundary layer effects on a stationary wind-blown fire. (Left) No boundary layer development surface, i.e. placed directly in the free-stream flow. (Right) 25 cm boundary layer development surface (boundary layer thickness ≈ 2 cm). The fuel source was a heptane-soaked wick and an inert surface was placed downstream for all experiments to observe attachment of the flame.

In order to investigate the mechanisms responsible for these instabilities, experiments were conducted on UMD's forced flow burner apparatus to see what flow configurations were necessary for the formation of streamwise streaks. After a series of experiments, it was found that the length of the flat, inert surface leading into the flame significantly modified observed structures in the flow. A 30 cm wide, 12 cm deep porous ceramic wick was soaked with heptane and ignited in a 1.3 ms^{-1} flow with

two different leading edge conditions. First, the wick was placed directly in the free stream flow, allowing for negligible boundary layer development. Second, the wick was placed parallel to the surface of the wind tunnel, providing an 8 cm boundary layer development length. Figure 3illustrates this effect with two different configurations. The difference in the flames is striking, the uniform flow generated flame with no boundary layer development has almost no observable streaks, with a flatter, more laminar appearance (left-hand side of Figure 3). The flame with the boundary layer, however, forms strikingly coherent streaks which periodically force the flames closer to the fuel surface (troughs) or further into the air (peaks) along the width of the burner. Analysis of the two configurations utilizing methods described in the proceeding sections also showed that the boundary-layer configuration results in higher burning rates (0.8 g/s vs. 0.3 g/s), measured by a load cell and higher flame fluctuation frequencies than the uniform-flow configuration (7.3 Hz vs. 3.5 Hz). Therefore, the formation of streaks appears to be important in understanding downstream heating and thus fire spread.

4.2. Streamwise Streak Analysis

Streamwise streaks were observed to originate at the base of flames where any boundary layer development was present, whether that development occurred due to external forced flows or entrainment into the flame on inclined experiments. Streaks are observable due to up wash regions (peaks) where flames illuminate the structure. In order to further understand the instability which modifies the spacing between these streaks, measurements of the streak spacing were taken under a wide variety of flow configurations. High speed video taken from the top of the experiments was used to determine this average streak spacing 1 cm from the base of the flame.

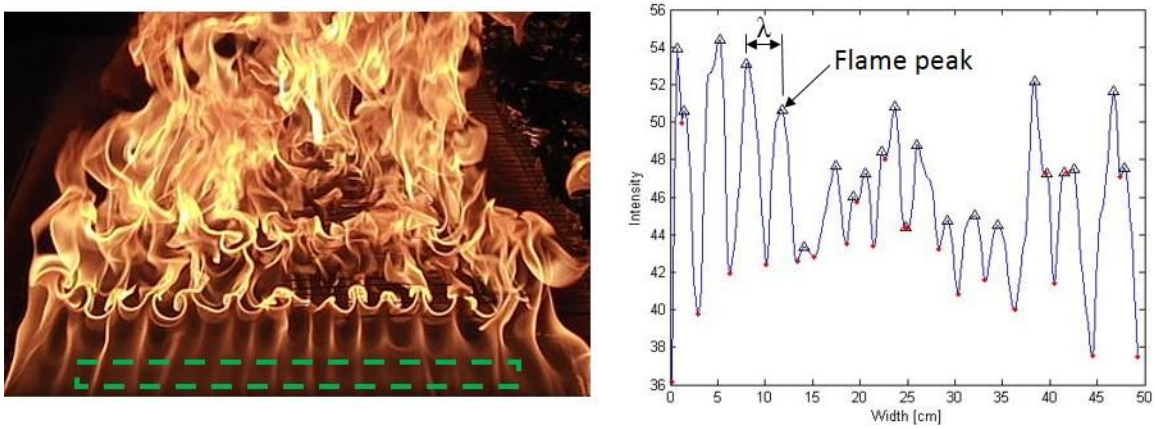

Figure 4. Streak analysis method for stationary gas burners. (Left) Top-view image from the Missoula inclined experiment, with a crop box region identified by dashed green lines. (Right) Smoothed intensity plot across the width of the burner, with local maximums marked as black triangles, representing the flame upwash peak.

The video was loaded into MATLAB and decomposed into individual frames. The region-of-interest started at the base of the flame across the width of the burner. For image analysis, the region was cropped one centimeter from the base of the burner in the flow direction. The intensity for each pixel column in the region-of-interest is averaged and the intensity across the width of the burner smoothed. The local maximums in intensity were determined to be a streak in the flow, and the spacing between the streaks determined for each image (Figure 4). Streak spacings for each experiment were then plotted on a histogram, fit to a log-normal distribution and the peak was used to scale the spacing between streaks for experiments (Figure 5).

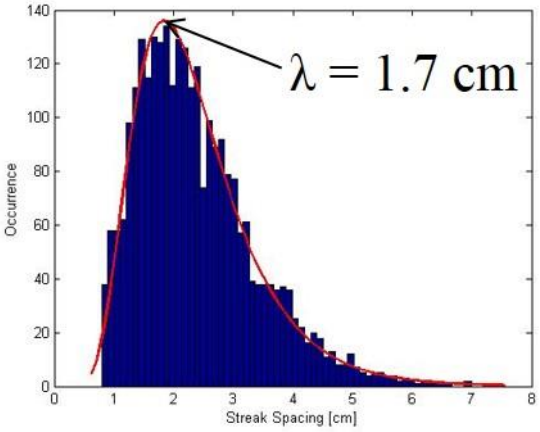

Figure 5. Probability distribution function (PDF) of streak spacing for a single experiment. The vertical axis represents the frequency of occurrence and the horizontal access the streak spacing observed. The red line indicates a log-normal distribution fit to the observed PDF.

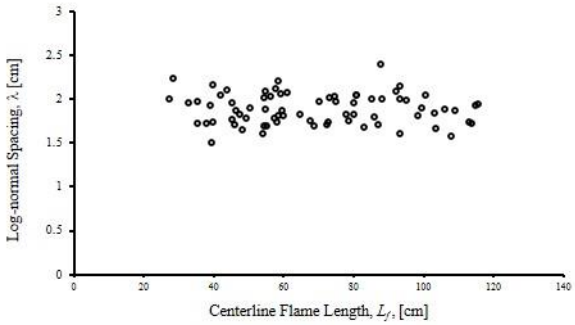

Figure 6. Maximum log-normal streak spacing, λ, remains relatively constant for small scale stationary burner experiments.

Similar to large scale experiments (Finney *et al*. 2013a), a relationship between the streak spacing and flame length were found, shown in Figure 6. This relationship appears nearly linear here over the limited test conditions, however if plotted against large-scale data (Finney *et al*. 2014) a relationship between flame length and streak spacing of the form, $\boldsymbol{\lambda = 0.39L_f + 0.34}$ is observed. While the streaks meander from side to side during tests, the uniformity of the log-normal distributions observed show that they are coherent in formation for the unique conditions of every test. Their formation requires incoming vorticity of both the boundary layer and flame to interact, forming a centrifugal instability similar to Taylor-Görtler vortex streaks. Other instabilities are also observed, especially in inclined experiments, namely span wise waves that appear on the base of the inclined burner. These are most likely Tollmien-Schlicting waves that form at the base of a boundary layer from small perturbations that slowly grow in size and play a critical role in a laminar flow's transition to turbulence (Goldstein and Hultgren 1989). In these observed boundary layers, these waves cause flames to break off into flamelets so that they are easily observable. Similar structures are also seen in larger spreading fire experiments in the 3×3 m Missoula wind tunnel (Finney *et al*. 2014). They may play a role in the formation of pulsations or bursts of flames discussed in the next section. Further research using stationary burners will explore more effective scaling techniques and ways of predicting their formation and effects.

4.3. Flame Pulsation Analysis

Pulsations, or bursts of the flame beyond the mean flame front location were observed in spreading fire experiments as well as in stationary burners (Figure 7). The flame location in stationary experiments was determined using side-view high-speed video and an array of thermocouples ahead of the burner. A region starting at the downstream edge of the burner and extending fully downstream, 1 cm above the surface was determined as a region of interest where extension of the flame would relate to flame attachment and fuel particle heating. The flame location was then determined in this region-of-interest by tracking the furthest-most downstream tip of the flame. This location fluctuated in time and it was observed that the flame would pulse downstream, "bursting" into what would be the unburned fuel region in a spreading fire experiment.

Experimental videos were loaded into a MATLAB script for analysis. The previously described region of interest was defined from the downstream edge of the burner surface to the end of the image in the downstream direction, with a height above the surface of 1 cm (see the dashed purple rectangle in Figure 7). Each image in the video was cropped to this same region-of-interest and then converted to a black and white image using the same average threshold value from the streak analysis. The attached flame location (xa) was determined as the furthest downstream pixel in the region-of-interest that satisfied the flame threshold level (Figure 7).

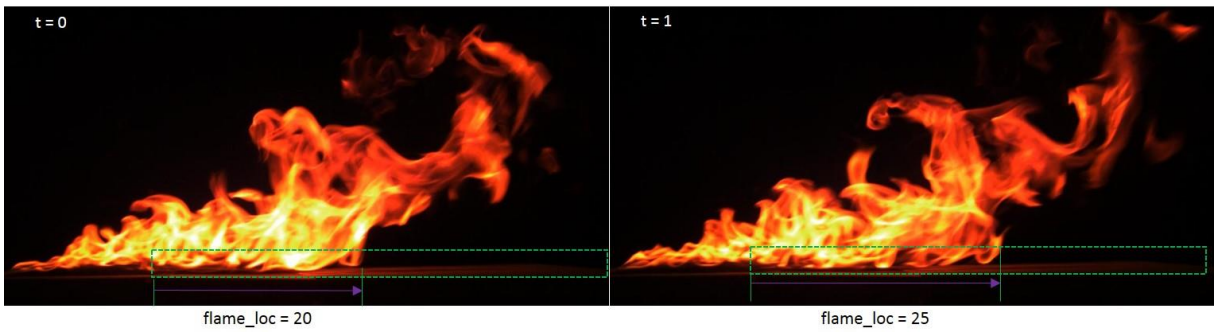

Figure 7: Flame location between two time steps in a forced flow experiment. The flame attachment location (x_a) is measured from the downstream edge of the burner to edge of the flame within the attachment region.

The flame extension downstream within the attachment region fluctuated in time, causing intermittent flame contact (Figure 8). The frequency of the flame pulsations was determined at locations on the downstream end of the burner using a variable interval time average (VITA) method (Blackwelder and Haritonidis 2006). The levels were determined at a range of locations downstream of the burner, starting at the burner edge and increasing in 1 cm increments (Figure 9). The flame position in time was compared to each of these locations and the number of occurrences was tallied. A level-crossing in the VITA technique was only considered for one direction; therefore only when the flame was previously not at a location and then at it in the next time step was it considered a crossing. The frequency for each location was then determined by dividing the number of crossings by the total number of frames analyzed, and multiplying by the frame rate of the video.

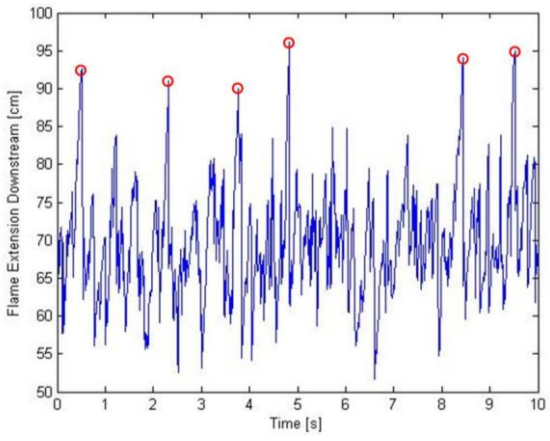

Figure 8. Flame location over time determined with high-speed videography. Flame location fluctuates around maximum frequency pulsation distance, but occasionally "bursts" further downstream (noted by red circles).

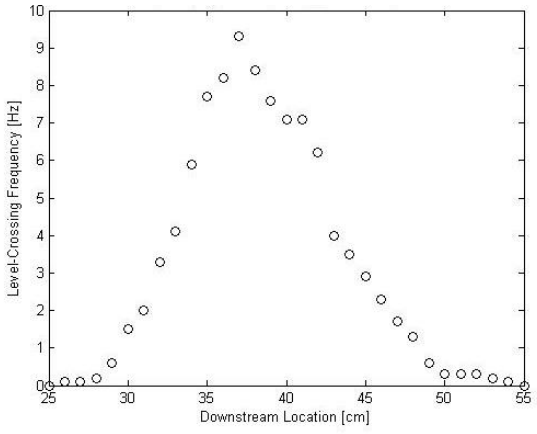

Figure 9. VITA frequency at advancing downstream locations.

In analysis of the trend of the frequency with different configurations, an analogy with pulsating pool fires was applied in the form of a Strouhal-Froude relationship. The Strouhal number, $\boldsymbol{St = fL/U}$, where *f* is the VITA frequency, *L* is a characteristic length scale and *U* is the free-stream velocity, was used to non-dimensionally relate oscillating flow mechanics to a balance of momentum and buoyancy forces. For this, the Froude number was used, $\boldsymbol{Fr = U/(gL)^2}$, where *g* is the acceleration due to gravity. Following the analysis of spreading fires (Finney *et al*. 2014), the flame length L_f was chosen as a characteristic length scale for the system, which represents the magnitude of the buoyant force. Figure 10 shows this scaling, $St = 2Fr^{-0.3}$ which is resolved from forced-flow gas burner experiments. The value of this exponent is below the value of -0.43 found in scaling for larger-scale fire spread experiments (Finney *et al*. 2014) and the -0.5 for diameter scaling of puffing in circular pool fires (Cetgen and Ahmed 1993 and Malalasekera *et al*. 1996). While the flame length may not be the most fundamental quantity for scaling analysis because of its coupling to experimental conditions, it is useful as most wildland fire spread analyses are correlated to this quantity (Byram 1959).

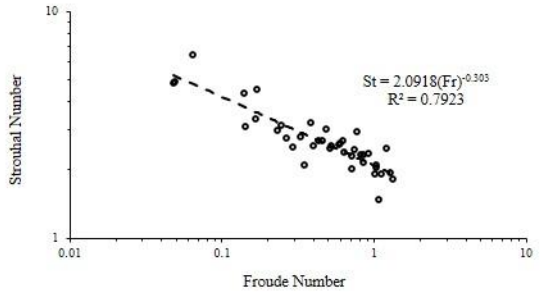

Figure 10. Strouhal-Froude scaling for stationary burners in forced-flow environment.

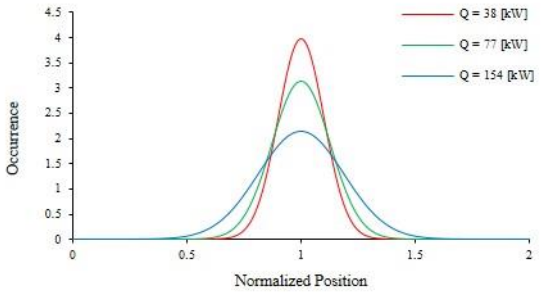

Figure 11. Probability-density function distribution of flame attachment along the free surface for three different heat-release rates (Q).

Statistical analysis of the flame position over time was also performed by producing a probability density function of the normalized flame attachment length (x_a) for different fire and flow configurations on an inclined and forced-flow gas burner. A histogram of the flame attachment length consistently shows a normal distribution of the downstream flame extension along the surface for each experiment. To compare the distribution for experiments, the attachment length was normalized with the average of the flame attachment distance in the attachment region (nominally an average flame extension along the free surface). The mean and standard deviation of the normalized flame location was then used to produce normal probability density functions, one of which is shown in Figure 11.
The representative tests shown in Figure 11 indicate increasing heat-release rates (Q = 38.6, 77.1 and 154.3 kW/m^2) of ethylene on the inclined Missoula flame wall. As the heat-release rate of the fire is increased, it is clear that the peak downstream extension of the flame resides further away from its mean position and extends further downstream more often. While other variables were compared, such as the incoming wind velocity and slope angle of inclined burners, once normalized with the flame length they were found to have little effect on the relationship shown in Figure 11. The implications of this finding are that, despite varying flow conditions and relative fire sizes (L_f), it is the overall heat-release rate of the fire that represents increasing extension of flames beyond the mean flame length into unburnt fuels. This perhaps suggests a means for correlation or future study.
Finally, an analysis was performed to investigate how far downstream of a burner a maximum VITA frequency would occur. Again, the relative fire size in terms of heat-release rates were found to best represent the variation in frequencies observed. Figure 12 shows this relationship, with the distance at which the maximum VITA frequency for a fire is observed downstream of a gas burner for various

inclined and forced-flow conditions versus a dimensionless fire size, $\boldsymbol{Q^* = Q/\left(\rho c_p T g^{1/2} L_f^{5/2}\right)}$, where $\boldsymbol{Q}$ is the heat-release rate of the fire, $\boldsymbol{\rho c_p T}$ representative gas density, specific heat and temperature, respectively, g acceleration due to gravity and $\boldsymbol{L_f}$ the flame length.

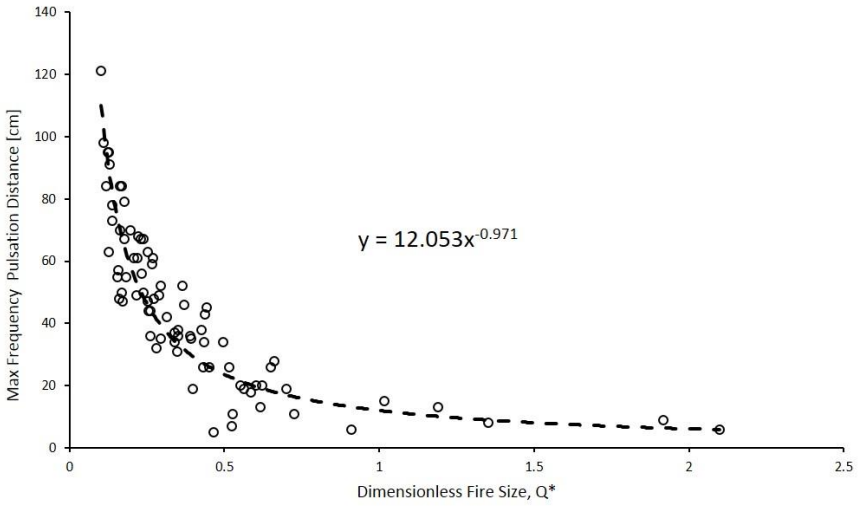

Figure 12. Max-frequency pulsation distance downstream into "unburnt fuel-bed" is considerably far for fires with low dimensionless fire size, Q*, and decreases exponentially with increasing dimensionless fire size.

4.4. Flame Geometry

Knowledge of the mean flame geometry, such as flame length, tilt angle, etc. are useful for assessing fire properties and can be easily obtained from stationary fire experiments. Measurements of the two-dimensional flame geometry were taken from side view images of the each experiment. Videos were processed into gray-scale images in MATLAB for the analysis. To determine the average flame geometry, the image was converted to RGB and all pixels with values between 0.48 and 0.52 were converted to red (Figure 13). To distinguish between flame and non-flame in the images, a thresholding tool was used on five randomly selected frames, from which a threshold was selected for the luminosity of the flame and background (non-flame). An average threshold value was then used for converting all frames in the video. Thresholding converted the gray-scale images to binary, black-and-white images, with 1 indicating flame and 0 indicating no flame. All images were then averaged.

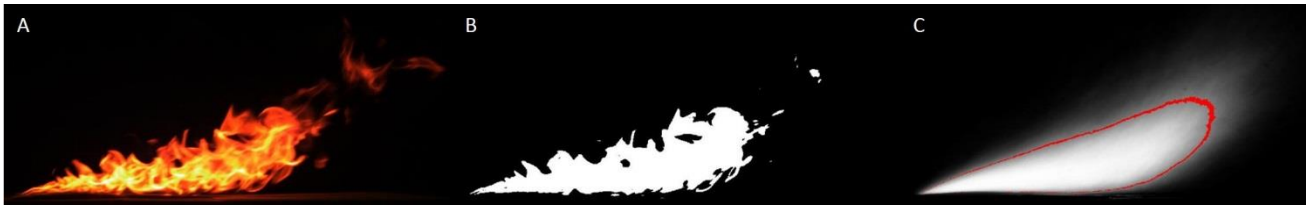

Figure 13. Image averaging technique used to determine flame geometry. (A) Still image from side-view camera (B) Black and white converted image using flame intensity threshold. (C) All black and white images averaged with pixel values between 0 and 1. A threshold line following pixels with value 0.48-0.52 are shown in red, identifying the average flame geometry.

Several flame geometry measurements were made using the average image (Figure 13 and 14). The flame tip was considered to be the highest point, furthest downstream from the burner. Flame length (L_f) was then measured from the midpoint of the burner (d/2) to the flame tip, along the centerline of the flame. The flame height (H_f) and flame extension (x_f) lengths were measured from the top of the

surface and the downstream edge of the burner to the flame tip, respectively. The attachment length (x_a) was defined as the average distance the flame extends downstream within the attachment region (denoted as a dashed box 1 cm above the attachment surface). The boundary-layer thickness incoming to the base of the burner (δ) was determined based on hot-wire anemometer measurements as 99% of the incoming free-stream fluid velocity, which compare favorably to estimates of δ using the Blasius solution (White 2011).

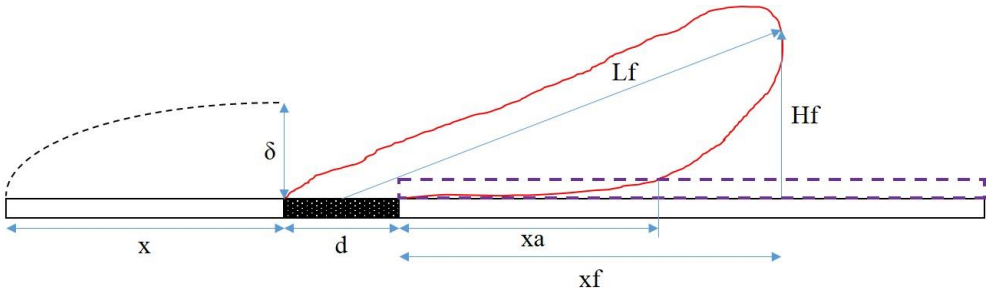

Figure 14. Physical length scales of the experiment. Independent parameters shown include the depth of the burner, d, leading edge, x, and boundary-layer thickness, δ. Dependent variables include the flame length L_f, flame height, H_f, flame length along the surface, x_f, and flame attachment length x_a.

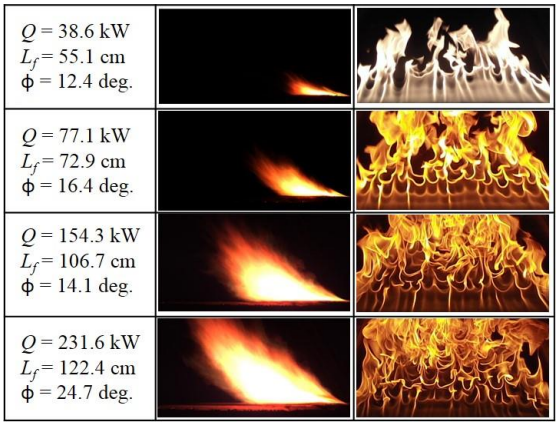

Figure 15. Variation of flame tilt angle based on heat release rate per unit length of the burner width (59.5 cm) at slope angle of 30 degrees. Burner depth = 12.7 [cm]

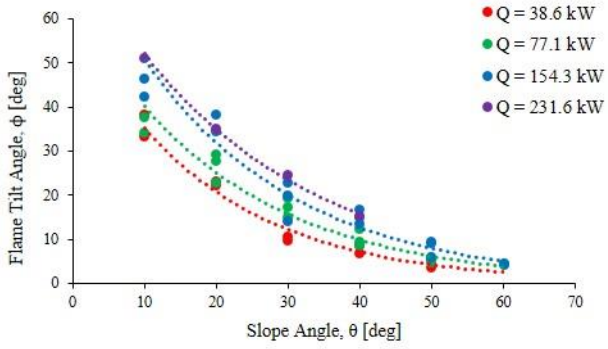

Figure 16. Flame tilt angle for several different heat-release rates (Q) on an inclined gas burner.

Figure 15 shows four representative conditions for tests on an inclined ethylene gas burner. Variations in the heat-release rate per unit length ($\dot{\boldsymbol{Q}}$), the flame length, $\boldsymbol{L_f}$ and the angle of inclination, $\boldsymbol{\phi}$ on the flame geometry are shown in both side-view and front-view images. From the side view, it can be seen that as both the angle of inclination and heat-release rate are increased, the flame length increases, however the attachment region does not experience a linear increase with flame length. The slope angle, which is representative of the attachment of the flame to the surface is shown in Figure 16. As the slope angle of the burner is increased, the flame tilt angle decreases, thereby signifying the flames becoming more and more attached to the surface of the burner. With increasing heat-release rates, it takes a greater angle of inclination for the flames to attach closer to the surface. This is expected as additional buoyant forces propel the flame upwards, compared to incoming entrained air.

A dimensionless length scale, $\boldsymbol{D^* = [\dot{Q}/(\rho c_p T g^{1/2})]^{2/5}}$ has been used in the fire research community to describe the source strength of a buoyant fire source (Quintiere 1989). This non-dimensional length

scale is given by the ratio of the fire heat release-rate $\dot{\boldsymbol{Q}}$ to the ambient air conditions $\boldsymbol{\rho c_p T}$ (density, specific heat, and temperature) and the square root of the acceleration due to gravity, all raised to the 2/5 power. The gravity term contributes to the buoyant force of the fire, and should act parallel to the line of action of the flame. To incorporate the slope angle of inclined fires, a rotated gravity vector term parallel to the inclined surface is used, given by the acceleration due to gravity time the sine of the slope angle. Flame lengths of pool fires, for instance, can be scaled with the dimensionless fire length, $\boldsymbol{D^*}$, and so with an adjusted gravity vector they should be able to as well. In Figure 17, preliminary scaling of the flame length with an adjusted gravity vector is shown to scale linearly with the centerline flame length. This suggests that the flame length for fires over sloped surfaces may be universally correlated if the correct ratios between buoyant forces and the gravity vector are taken into account.

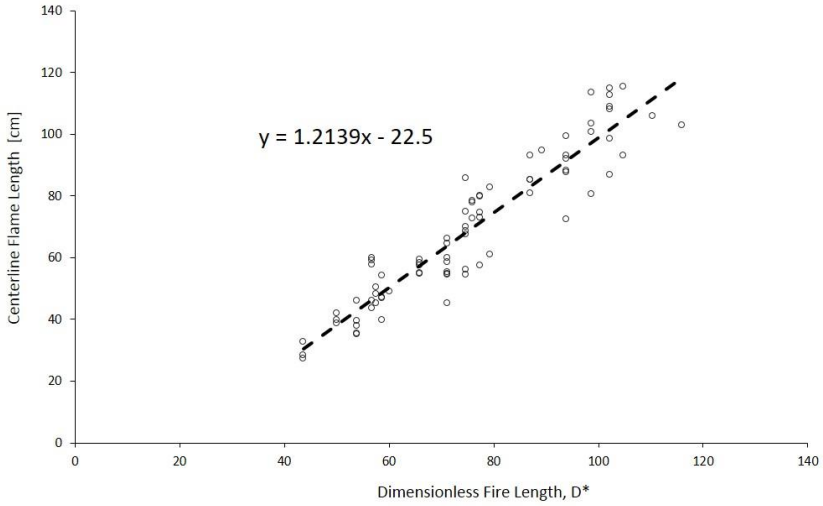

Figure 17. Relationship between centerline flame length and dimensionless fire length parameter D*, shows that for larger fires in steep slope the flame length is increases linearly.

5. Conclusions

This study has presented a framework for the use of stationary gas burners to study spreading wildland fire behavior, enabling measurements and analysis of key parameters related to instabilities and flame geometry that play a role in flame spread. Numerous techniques used to accomplish this are shown, as well as preliminary scaling analysis. Recently-discovered instabilities and flow structures are shown to be re-created in steady gas burners, allowing for more detailed studies, including statistical analysis made possible by the long time scales stationary flames can be created. Correlations for the mean flame geometry, such as the flame tilt angle and flame length can also be obtained by these studies with appropriate nondimensional scaling.

6. References

Atkinson, G., Drysdale, D. & Wu, Y., 1995. Fire driven flow in an inclined trench. *Fire safety journal*, 25.

Blackwelder, R. F., & Kaplan, R. E. (2006). On the wall structure of the turbulent boundary layer. *Journal of Fluid Mechanics*, *76*(01), 89.

G.M. Byram, Combustion of forest fuels. In: Davis, K.P., ed. Forest fire: control and use., New York McGraw Hill. (1959) 61–89.

Cetegen B. and T. Ahmed, Experiments on the periodic instability of buoyant plumes and pool fires, *Comb. Flame,* pp. 157-184, 1993

Clark, T.L., L. Radke, J. Coen, and D. Middleton. 1999. Analysis of Small-Scale Convective

Dynamics in a Crown Fire Using Infrared Video Camera Imagery. J. Appl. Meteorology. 38:1401-1420.

Finney, M.A., Forthofer, J. and Grenfell, I., 2013a. A study of flame spread in engineered cardboard fuelbeds; part I: Correlations and observations. *Seventh International Symposium on Scale Modeling (ISSM-7) Hirosaki, Japan, August 6-9, 2013.*

Finney, M.A. *et al*., 2013b. On the need for a theory of wildland fire spread. *International Journal of Wildland Fire*, 22(1), p.25.

Finney, M.A. *et al*., 2010. Structure of Diffusion Flames from a Vertical Burner. *IV International Conference on Forest Fire Research D.X. Viegas (Ed.), 2010.*

Finney, M.A. Cohen, J., Forthofer, J., McAllister, S. Adam, B. Akafuah, N., English, J., Saito, K., Gollner, M.J. and Gorham, D., Experimental Evidence of Buoyancy Controlled Flame Spread in Wildland Fires. VII International Conference on Forest Fire Research, Coimbra, Portugal, 14 to 20 Nov, 2014.

Goldstein, M. E., and Lennart S. Hultgren. "Boundary-layer receptivity to long-wave free-stream disturbances." *Annual Review of Fluid Mechanics* 21.1 (1989): 137-166.

Jeschke, P. & Beer, H., 2001. Longitudinal vortices in a laminar natural convection boundary layer flow on an inclined flat plate and their influence on heat transfer. *Journal of Fluid Mechanics*, 432, pp.313–339.

Jimenez, D., Finney, M.A. & Cohen, J., 2010. Design and Construction of Gas-Fed Burners for Laboratory Studies of Flame Structure. *IV International Conference on Forest Fire Research D.X. Viegas (Ed.), 2010.*

Malalasekera, W.M.G., H.K. Versteeg and K. Gilchrist. 1996. A review of research and an experimental study on the pulsation of buoyant diffision flames and pool fires, *Fire and Materials*, vol. 20, no. 6, p. 261-271

Oka, Y. *et al*., 2000. Modelling Of Unconfined Flame Tilt In Cross-Winds. *Fire Safety Science*, 6, pp.1101–1112.

de Ris, J. and Orloff, L., 1975. The role of buoyancy direction and radiation in turbulent diffusion flames on surfaces. *Symposium (International) on Combustion*, 15(1), pp.175–182.

Saric, W.S., 1994. Gortler vorticies. *Annual Review of Fluid Mechanics*, (2), pp.379–409.

White, F.M., 2011. *Fluid Mechanics* 7th ed., New York, NY: McGraw Hill.